



Research article

Exploring *Elaeis guineensis*: Enzyme inhibition, antimicrobial properties, chemical composition and *in silico* docking analysis

Ateeq Ahmed Al-Zahrani^{1,*}, Mustapha Abdullahi², Abdulrahman Mahmoud Dogara^{3,*}, Abubakar Abdullahi Lema⁴, Muhammad Tukur Ibrahim⁵, Aisha Abdullahi Mahmud⁶, Muhammad Usman⁷ and Ammar A. Razzak Mahmoud⁸

¹ Chemistry Department, University College at Al-Qunfudhah, Umm Al-Qura University, Saudi Arabia

² Faculty of Physical Sciences, Department of Pure and Applied Chemistry, Kaduna State University, Tafawa-Balewa Way, Kaduna State, Nigeria

³ Biology Education Department, Tishk International University, Erbil, Iraq

⁴ Department of Biological Sciences, College of Natural and Applied Sciences, Al-Qalam University Katsina, Katsina, Katsina State, Nigeria

⁵ Department of Chemistry, Ahmadu Bello University, P.M.B. 1044 Zaria, Kaduna State, Nigeria

⁶ Department of Plant Science and Biotechnology, Faculty of Life Science, Federal University Dutsin-Ma, Katsina State, Nigeria

⁷ Department of Biotechnology, Faculty of Science, Nigerian Defense Academy, Kaduna, Nigeria

⁸ Department of Pharmaceutical Chemistry, College of Pharmacy, University of Baghdad, Iraq

* **Correspondence:** Email: aaalzahrani@uqu.edu.sa, abduallahman.mahmud@tiu.edu.iq; Tel: +966547393953, +2348036437378.

Abstract: For centuries, plants have been essential sources of food, shelter, and traditional medicine. With growing antimicrobial resistance and the side effects of modern drugs, there is an urgent need to explore natural remedies as safer therapeutic alternatives. Thus, we aimed to evaluate biological activities, chemical composition, and molecular docking of *Elaeis guineensis*. Total phenolic content (TPC), total flavonoid content (TFC), radical scavenging activity (DPPH), ferric reducing antioxidant potential (FRAP) assay, α -glucosidase, antimicrobial, gas chromatography mass spectrometry (GCMS), and molecular docking were evaluated. The findings showed average values of 85.23% for DPPH, 57.2 mg/g dry weight for ferric FRAP, 140.4 mg/g Gallic Acid Equivalents for TPC, 120.2 mg/g Quercetin Equivalents (QE) for TFC, along with $65.01 \pm 0.2\%$ for α -glucosidase and 14.2 ± 0.2 mm for

antimicrobial activity from the ethanol peel extracts. The virtual docking screening showed that compounds 8, 10, and 14 had better binding scores with MolDock scores between -106.05 and -108.94 kcal/mol than that of ciprofloxacin (-105.84 kcal/mol), with hydrogen and hydrophobic bonds playing the most crucial contributions in the molecular interactions. These combined *in vitro* and *in silico* findings imply that the peels of *E. guineensis* are rich in multifunctional phytochemicals that exhibit strong antioxidant, α -glucosidase, and antibacterial inhibitory properties.

Keywords: *Elaeis guineensis*; flavonoids; antimicrobial activity; *in-silico*; virtual docking

1. Introduction

Medicinal plants have been a part of humanity's concern for its overall wellness for centuries, providing a range of naturally derived drugs for many ailments [1]. As a result of increased worldwide medical concern about antibiotic resistance and secondary actions of synthetic drugs, a new demand for therapeutic compounds with a plant origin emerges [2]. *Elaeis guineensis* (*E. guineensis*), a commercially produced and economically significant species with documented pharmacologic activity, including antioxidant, antimicrobial, and anti-inflammatory activity, is one such species. Despite its fruit's extracted oil being commercially utilized in foods and cosmetics, its phytochemical profile and therapeutic potential have not become a field of continuous scientific inquiry [3].

E. guineensis (oil palm), which is known historically as oil palm, grows naturally in West Africa territories primarily because of its edible fruit. The fruit bunches of the tree contain palm oil seeds that are extracted for production [4]. The plant *E. guineensis* holds significant economic value worldwide because palm oil derived from its fruit serves multiple purposes in manufacturing food products and cosmetics along with biofuels and pharmaceutical applications [4,5]. Traditional medical practitioners have used *E. guineensis* to treat dysmenorrhea, poison, convulsions, skin troubles, colds, persistent coughs, malaria, fibroids, diabetes, and microbial infections because its oil controls blood sugar, and its antimicrobial properties help in treating wounds and infections [6].

Antimicrobial resistance [7] has risen immensely, lowering the efficacy of conventional antibiotics such as ciprofloxacin, and, therefore, alternative therapeutic compounds have been in demand ever since [8]. DNA gyrase, an important bacterial enzyme for bacterial DNA replication, is an established target for antibacterial drug development. Compounds derived from conventional medicinal herbs have displayed strong potential in inhibiting bacterial DNA gyrase and, therefore, can serve as potential candidates for antimicrobial drugs [9–11].

Advances in computational biology have made powerful tools available for drug discovery, including molecular docking and molecular dynamic [12] simulations, increasingly accessible [13,14]. The underutilized peel of *E. guineensis* in Africa was targeted based on the evidence of its high phytochemical, hypothesizing that synergistic effects of bioactive compounds may overcome microbial resistance mechanisms. While the antioxidant and antimicrobial properties of *E. guineensis* extracts have been established, we provide a significant advancement by employing a multi-assay *in vitro* approach combined with computational evaluations of its peel-derived phytochemicals.

2. Materials and methods

2.1. Plant identification

The plant species was confirmed and determined by a qualified botanist at Botany Department Faculty of Science, Ahmadu Bello University. Herbarium collections of *E. guineensis* (vouchers ABU09634) were prepared and deposited. Species determination was achieved with World Flora Online (WFO) at <https://www.worldfloraonline.org/>.

2.2. Plant sample extraction and determination of % yield

The peels of *E. guineensis* were initially rinsed under running water to eliminate any extraneous materials. Following this cleaning process, the peels were dehydrated and subsequently ground into a fine powder with the aid of a grinding machine, with each sample weighing 100 g. Soxhlet extraction was conducted utilizing four distinct solvents: Ethanol, water (aqueous), hexane, and acetone. Post-extraction, the filtrates were filtered through Whatman No. 1 filter paper. The extracts obtained were then concentrated using an E-Z-2 Elite evaporator, with the operational temperatures adjusted according to the boiling points of the respective solvents: Ethanol at 72 °C, water at 100 °C, hexane at 55 °C, and acetone at 56 °C. The final concentration of the extracts was achieved by drying them in a vacuum oven at 40 °C until a stable weight was reached [3]. The weight of the crude yield was derived through calculation: $\text{Yield \%} = \text{Extraction yield (\%)} = F1/F2 \times 100$, whereby F1 = Mass of the crude extract and F2 = Mass of the sample [15].

2.3. Determination of total phenolic content (TPC)

After the incorporation of 1.5 mL of reagent grade Folin-Ciocalteu reagent into 200 µg of crude extract, the mixture was incubated for two hours in a controlled light condition. A spectrometer was utilized to determine the absorbance at 750 nm, which was subjected to gallic acid at different doses (Figure 1). The results were expressed in milligrams of gallic acid equivalent per gram of dry weight (DW) based on the gallic acid standard curve equation, $y = 0.0052x + 0.0135$, with $R^2 = 0.9693$ [16].

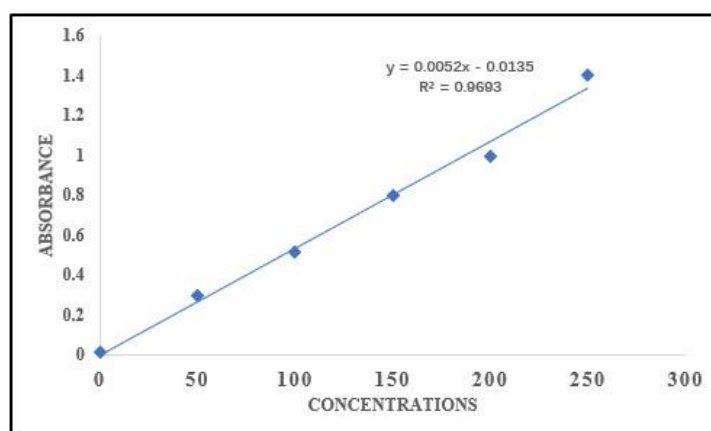


Figure 1. Standard curve for total phenolic content.

2.4. Determination of total flavonoid content (TFC)

A total of 4 mL of water, 0.3 mL of 5% sodium nitrate, and 1 mL of extract was blended. This is preceded by the addition of 2 mL of 1 M sodium hydroxide, 2.4 mL of water, and 0.3 mL of 10% aluminum chloride, the mixture incubated for 15 minutes. Absorbance was measured with a spectrophotometer set at 510 nm in terms of wavelengths, with 25 mg of quercetin samples at different concentrations (Figure 2). The following was expressed as a function of mg of Quercetin Equivalents (QE) per g of DW, and its respective values were fitted onto a normalized curve of Quercetin with $y = 0.0138x + 0.0085$, with an $R^2 = 0.9981$ [17].

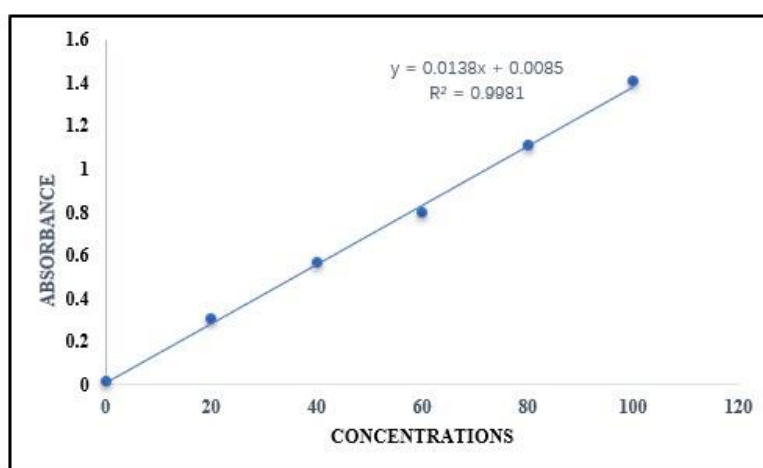


Figure 2. Standard curve for total flavonoid content.

2.5. Radical scavenging activity DPPH

The efficacy of the extracts in neutralizing the free radical DPPH was obtained. The reaction was conducted in a 96-well microplate utilizing 40 μ L of each extract at various concentrations and 160 μ L of a DPPH radical solution, dissolved in 1 mM in methanol. The combination was incubated at ambient temperature and under darkness for 30 minutes. The absorbance was measured using a microplate reader at 517 nm. The samples' ability to eradicate DPPH was assessed using their inhibition percentages, computed using the subsequent equation:

$$\% \text{ of inhibition} = [(AR - (H - AH)) / AR] \times 100$$

where AR = Absorbance of reagent blank, H = Absorbance of samples, and AH = Absorbance of blank sample [18].

2.6. Ferric reducing antioxidant potential (FRAP) assay

Preparations were made for stock solutions consisting of 10 mL of acetate buffer with a pH of 3.6, 1 mL of TPTZ (2,4,6-tripyridyltriazine) solution in hydrochloric acid, and 1 mL of FeCl_3 solution. A total of 100 μ L of crude extract and 300 μ L of de-ionized water were added with 3 FRAP solution. This was incubated and mixed in a 37 $^{\circ}\text{C}$ water bath for a duration of 30 minutes duration. Ascorbate

acid was used in this investigation as a positive control. The spectrophotometer was used to record the absorbance of the produced solution at a 594 nm wavelength, with buffer serving as a blank. A standard curve was generated using a series of $\text{FeSO}_4 \cdot 7\text{H}_2\text{O}$ concentrations. The curve equation was $y = 0.0003x + 0.098$, and its R^2 value was 0.9961. The results were determined in terms of milligram Ascorbic Acid Equivalent (AAE) per gram of dried matter (DW) [19].

2.7. α -glucosidase inhibition assay

A total of 10 μL of the extract at 100 $\mu\text{g/mL}$ was combined with 50 μL of 0.1 M phosphate buffer (pH 7.0), followed by the addition of 25 μL of α -glucosidase in 0.2 U/mL buffer to the well plate, which was then incubated for 10 minutes at 37 °C to commence the reaction. A total volume of 25 μL of 0.5 mM 4-nitrophenyl alpha-D-glucopyranoside (pNPG) substrate was incorporated to finalize the reaction, and the mixture was incubated for an additional 30 minutes at 37 °C. The reaction was concluded by the addition of 100 μL of 0.2 M sodium carbonate solution. Acarbose served as a positive control. The absorbance was quantified at 410 nm [20]. The % of inhibition was determined via the following formula: % of inhibition was determined as $\text{inhibition (\%)} = [\text{Control abs} - \text{sample abs}] / \text{control abs} \times 100$.

2.8. Evaluation of antimicrobial activity

2.8.1. Test organisms

Gram-negative (*S. Typhi*) were obtained from the Biological Sciences Department at Al-Qalam University, Katsina, Katsina State. The microbial stock cultures were inoculated onto Mueller–Hinton agar plates using an inoculation loop. The plates were incubated for 24 hours at 37 °C. The following day, they existed as a subculture until a new colony emerged. Subsequently, they were administered Mueller–Hinton broth and incubated at 200 rpm overnight.

2.8.2. Disk diffusion method

Microbial inoculums of 1.10^6 CFU/mL were sown on 200 μL solidified Mueller–Hinson plates. Plant extracts (ethanol, aqueous, acetone, and hexane) were applied at a concentration of 4000 $\mu\text{g/mL}$ using 25 μL on Whatman No. 1 filter paper discs measuring 6 mm in diameter. By applying sterile forceps, the infused disk was placed on the plate. The plates were then incubated at 37 °C for 24 hours [21]. Ampicillin (10 μg) (Positive control) and DMSO (Negative control).

2.8.3. Agar well diffusion method

Agar well diffusion method was used in a complementary way to assess how effectively the extracts diffuse. Microbial inoculums at 1.10^6 CFU/ml were sown evenly across 200 μL solidified Mueller–Hinton agar plates. Whatman No. 1 filter paper discs (6 mm) received 25 μL of extract solution prepared at 4000 $\mu\text{g/mL}$ concentration from plant material extracted with ethanol, aqueous, acetone, and hexane [22]. Ampicillin (10 μg) was the positive control and DMSO was the negative control. The plates were incubated at 37 °C for 24 hours. This method was complemented with the disk method to

evaluate extract potency and maintain consistency in antimicrobial assessments across diffusion techniques.

2.9. GC-MS-based identification of compounds

The ethanolic crude extract was analyzed using mass spectrometry (GC-MS, Shimadzu/QP2010) with an OV-5 bonded column measuring 30 m in length, 0.25 mm in diameter, and a 0.25 m thick film. Helium was utilized for propellant gas and reached about 1.0 mL/1 min flow rate and temperatures of 220 and 240 °C in the injector and detector, respectively, injecting 1.0 µL with a 1:20 split ratio. Temperature in the oven increased by a slow rise, starting at 60 °C to 240 °C at a velocity of 3 °C/1 min. The collected particles exhibited a velocity range of 40 to 650 m/s and an impact energy of 70 eV. The chemical constituents were discovered by cross-referencing them with an extensive database. In electron-impact mode, spectra were acquired with a scan range of 40–550 amu, an ionization energy of 70 eV, and a scan rate of 0.34 seconds. The quadrupole temperature and ion source temperature were 150 °C and 280 °C, respectively [23].

2.10. *In-silico studies*

2.10.1. Virtual docking screening of identified compounds

Molecular docking screening was performed using Molegro Virtual Docker (MVD) to appraise the residual interaction between the identified compounds in the extracts and the DNA gyrase subunit A (GyrA) from *S. Typhi*. The three-dimensional crystal structure of the GyrA with PDB code 5ZTJ was retrieved from the protein data bank repository website at <https://www.rcsb.org/structure/5ZTJ>. The retrieved protein was initially prepared by assigning bonds, bond orders, hybridization, charges, and explicit hydrogen atoms if missing in the protein structure using MVD [24,25]. Subsequently, the optimum detected active cavity was set within a constraint sphere of 15 Å radius with a center axis of X: 26.50, Y: 23.70, and Z: 24.79. The binding scores (MolDock scores) from the docking simulations were reported in comparison to ciprofloxacin, while the top protein-ligand complexes were visualized using Discovery Studio Visualizer 2020.

2.10.2. Molecular dynamic simulations

Molecular dynamic simulations were conducted for the top selected ligand-protein complexes with low binding energy during our docking studies. The simulations were performed using Desmond Simulation Software (Schrödinger). Each complex was solvated in a 10 Å explicit water box with periodic boundary conditions (PBC) employing the SPC water model [26–28]. The OPLS3e force field was utilized, and Na⁺ and Cl[−] ions were added to neutralize the system's overall charge. The system was initially subjected to 2000 steps of energy minimization before proceeding to a 200 ns production run. Prior to this, a brief 100 ps equilibration under isothermal-isobaric (NPT) conditions was conducted at constant pressure and temperature. During the NPT equilibration phase, the temperature was maintained at 300 K using the Nose-Hoover chain thermostat, and the pressure stabilized at 1.0315 bar using the Martyna-Tobias-Klein barostat [29–31]. The 200 ns simulation captured trajectory snapshots every 100 ps for analysis. Thereafter, to evaluate the binding stability, structural

characteristics, and overall system convergence of the selected complexes during the molecular dynamic [12] simulations, the resultant MD trajectories were subjected to a comprehensive analysis. This involved the calculation of several standard simulation parameters, including root mean square deviation (RMSD), root mean square fluctuation (RMSF), and hydrogen bond analysis. By examining these parameters, the dynamic behavior of the ligand-protein complexes was thoroughly investigated, providing valuable insights into their stability and structural integrity under simulated physiological conditions.

2.11. Prediction of antibacterial effectiveness

The antibacterial properties of the 15 compounds isolated from *E. guineensis* were evaluated against various microbial species using the AntiBac-Pred server [32]. This server employed a training dataset that included structural data for 41,065 chemical compounds, enabling the classification of drug-like molecules as either “active” or “inactive” concerning 353 bacterial strains. Compounds with minimum inhibitory concentrations (MICs below 10,000 nM) were designated “active”. The compounds were input into the server in SMILES format. A compound was chosen if its *Pa* value was greater than 0.5 to ensure a significant probability of activity. The *Pa* value ranged from 0, indicating inactivity, to 1, indicating complete activity. To represent the antibacterial activity data visually, a heatmap was constructed using Python (version 3.x, available at: <https://www.python.org/>). The libraries Matplotlib and Seaborn were employed for this purpose. The data were organized in a tabular format through the use of Pandas, facilitating the display of the antibacterial effectiveness of compounds across multiple bacterial strains. Bacterial strain names were italicized, and those that were resistant were marked as “Resistant”. Additionally, the compounds and bacterial strains were highlighted in bold for improved clarity.

2.12. ADMET profiling

The absorption, distribution, metabolism, excretion, and toxicity (ADMET) profiles of selected ligands were predicted using an effective machine learning web server, ADMETLab 3.0, at <https://admetlab3.scbdd.com/>.

2.13. Statistical analysis

All experiments were performed in triplicate, and the findings are expressed as mean \pm standard deviation (SD) using g Statistical Analysis System (SAS) software (University version 9.4). Statistical significance was evaluated using one-way analysis of variance (ANOVA). $p < 0.05$ was deemed statistically significant.

3. Results and discussion

3.1. Extract yield

The extraction properties between peel extracts demonstrate considerable differences in solvent extraction abilities. Among all peel extracts, the aqueous extract achieves maximum extraction

efficiency of 21% because its polar nature permits extraction of multiple plant compounds effectively. The 14% yield rate from ethanol peel extracts indicates that ethanol effectively extracts polar along with non-polar compounds. The acetone peel extract yields 9%. Hexane extract shows the minimum extraction yield at 8% due to its main focus on extracting non-polar substances while neglecting bioactive plant components. The extraction method and solvent characteristics with present chemical types and metabolite polarity strongly affect extraction yield from different parts of medicinal plants [22]. The extraction outcomes demonstrate how selecting the appropriate solvent affects extraction yield rates, as aqueous and ethanol extract are better compared to acetone and hexane for this plant material.

3.2. Antioxidant, enzyme inhibition, and antimicrobial activities

The antioxidant activity of *E. guineensis* extract was evaluated using the DPPH and FRAP free radical scavenging assay. The results reveal a concentration-dependent increase in antioxidant activity. At the highest concentration assessed, the extract exhibits 85% DPPH radical scavenging activity, which is comparable to the activity of quercetin, a standard antioxidant used in the study (Table 1). This high antioxidant potential can be attributed to the rich presence of phenolic and flavonoid compounds, which are well-known for their free radical scavenging abilities [33]. The antioxidant potential of *E. guineensis* extract is significant because oxidative stress is a key contributor to various chronic diseases, including cardiovascular disease and diabetes. Moreover, the extract's ability to neutralize free radicals highlights its potential for therapeutic applications in managing oxidative stress-related disorders [34].

Table 1. Antioxidant, α -glucosidase, total flavonoid, total phenolic, and antimicrobial activity of *E. guineensis* extract.

S/ N	Sample name	DPPH	FRAP	α -glucosidase	TFC	TPC	Antimicrobial		
		Inhibition %	mg/g dw				mg/g GAE	Disc	Agar well
1	Ethanol peel	85.23 ± 0.2^b	57.2 ± 1.2^a	65.01 ± 0.2^a	120.2 ± 1.2^a	140.4 ± 0.6^a	14.2 0.2 ^a	±	13.9 ± 0.7^a
2	Aqueous peel	78.5 ± 0.5^c	50.2 ± 0.9^b	52.16 ± 0.5^c	98.4 ± 2.2^b	111.2 ± 1.2^b	11.7 0.4 ^b	±	11.3 ± 0.2^c
3	Acetone peel	67.47 ± 0.4^d	43.2 ± 2.0^c	48.94 ± 0.4^d	84.6 ± 1.2^c	102.2 ± 1.4^c	-	-	-
4	Hexane peel	56.91 ± 0.7^e	35.4 ± 0.8^d	47.21 ± 0.6^e	76.5 ± 1.3^d	88.5 ± 1.2^d	11.0 0.3 ^c	±	10.1 0.1 ^d
5	Que/Acar /Amp	87.71 ± 0.3^a		58.64 ± 0.1^b			13.9 0.6 ^a	±	12.6 0.9 ^b

Note: Que; Quercetin, Acar; Acarbose, and Amp; Ampicillin (10 μ g). At $p < 0.05$, values with the same alphabet horizontally have no significant difference.

The α -glucosidase inhibitory activity of *E. guineensis* extract was assessed as a measure of its potential for managing type 2 diabetes by inhibiting carbohydrate digestion and absorption. The extract demonstrates significant inhibitory activity (Table 1), with an inhibition value of 65.01%, compared

to the standard drug acarbose, which has value of 58.64%. This suggests that *E. guineensis* extract possesses moderate α -glucosidase inhibitory properties, making it a potential natural alternative to synthetic drugs used for diabetes management [35]. The α -glucosidase inhibition is likely due to the presence of flavonoids and phenolic compounds, which have been documented to inhibit enzymes involved in carbohydrate metabolism, thus lowering postprandial blood glucose levels [35].

The total flavonoid content of *E. guineensis* extract was determined using a colorimetric assay and expressed as milligrams of quercetin equivalents per gram of dry extract (mg QE/g). The results indicate that a total flavonoid content of 120.2 ± 1.2 mg QE/g of ethanol extract has significant TFC, while Hexane has lower TFC 76.5 ± 1.3 (Table 1). Flavonoids are a diverse group of phytonutrients known for their antioxidant, anti-inflammatory, and anti-cancer properties [16]. The high flavonoid content of *E. guineensis* extract may contribute to its observed antioxidant and α -glucosidase inhibitory activities. Flavonoids are known to play a significant role in reducing oxidative stress and modulating carbohydrate metabolism, making them beneficial in the prevention and management of diseases such as diabetes and cancer [16]. The total phenolic content of the extract was measured using the Folin-Ciocalteu method and expressed as milligrams of gallic acid equivalents per gram of dry extract (mg GAE/g). The total phenolic content is significantly higher, 140.4 ± 0.6 mg GAE/g, in ethanol extract. Phenolic compounds are widely recognized for their antioxidant properties as they can donate hydrogen atoms to neutralize free radicals [36]. The relatively high phenolic content of the *E. guineensis* extract further supports its strong antioxidant activity, as phenolics are key contributors to scavenging reactive oxygen species (ROS).

The peel ethanol extract shows the highest antibacterial activity with the minimum inhibitory concentration of 620 μ g/mL on the tested bacterium, but it is weaker than the standard drug Ampicillin (Figure S1). Ethanol is a broad-spectrum (Figure 3) solvent that has been shown to extract a variety of polar and moderately polar bioactive compounds, including polyphenols, flavonoid and tannins, which are well-established in antimicrobial effects. Researchers have demonstrated that ethanol extracts from plant materials show better antimicrobial abilities to combat *S. Typhi*, as demonstrated by the ethanol peel extract results in our research. A study conducted by Stanislaus, Etsuyankpa [37] showed that ethanol extracts from *Allium sativum* and *Azadirachta indica* inhibited *S. Typhi* bacteria, thus proving ethanol effectiveness as a bioactive compound extraction solvent. According to Mahmood, Ashraf [38] *C. limon* and *Punica granatum* extracts in ethanol and acetone showed the greatest inhibition zones against *S. Typhi* bacteria which coincides with our observation of enhanced zone inhibition from ethanol-based extracts. Research findings demonstrate that selection of the proper solvent plays a critical role in establishing how plant extracts can act against microbial agents. Differences in bioactive compound solubility seem to be responsible for inhibition zone variations since ethanol works more efficiently than other solvents to extract antimicrobial compounds. The method of application through discs or agar wells along with the variable concentration of active compounds across extracts seem to affect the observed differences in effectiveness.

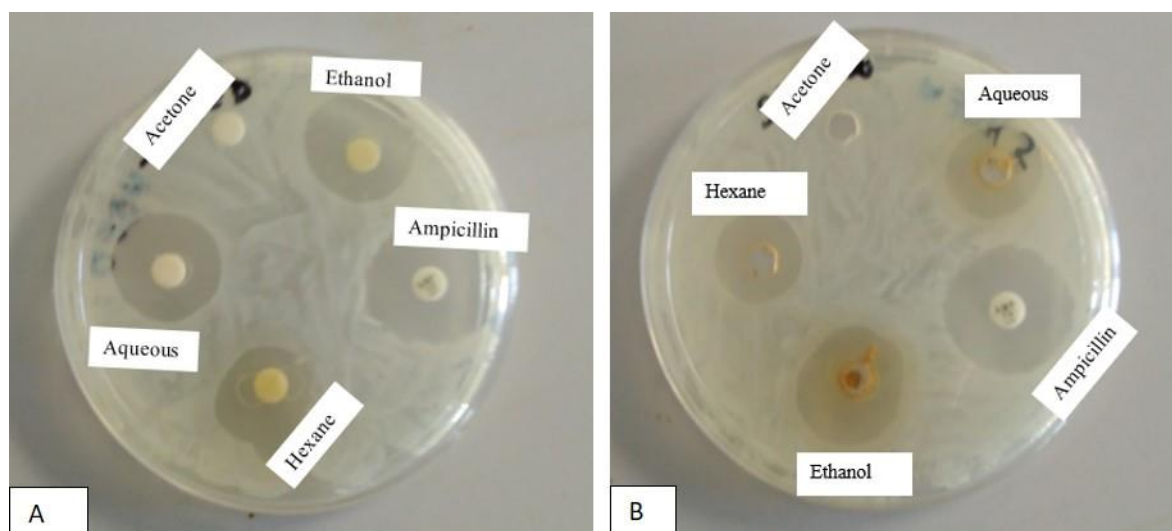


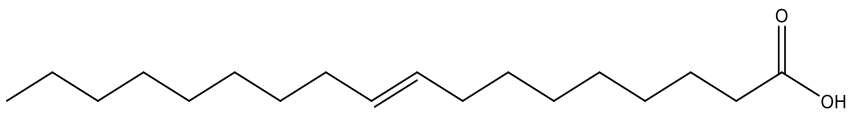
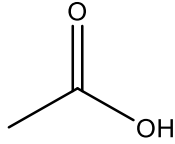
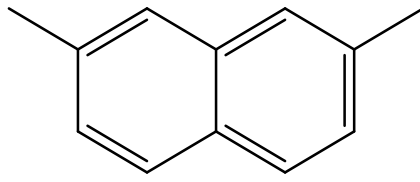
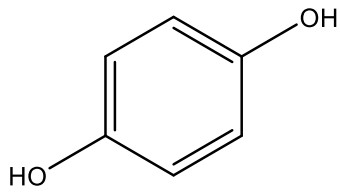
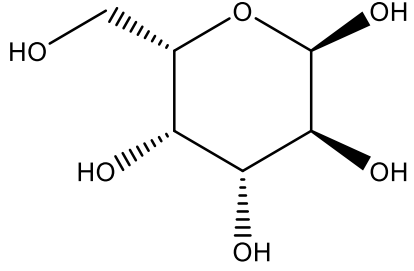
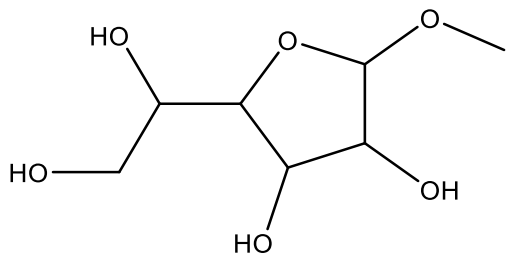
Figure 3. Sensitivity test of antimicrobial activity of *E. guineensis* extract. (A) Disc diffusion assay, and (B) ager well diffusion assay.

The antimicrobial activity can be attributed to the presence of bioactive compounds, such as flavonoids and phenolics, which have been reported to possess strong antimicrobial properties. These compounds disrupt bacterial cell membranes, inhibit enzyme function, and interfere with bacterial metabolism, leading to cell death [39]. The antimicrobial potential of *E. guineensis* suggests its usefulness in the development of natural antimicrobial agents, particularly in the fight against antibiotic-resistant bacterial strains [39]. The study demonstrated that *E. guineensis* extract possesses significant antioxidant, α -glucosidase inhibitory, and antimicrobial activities. The high levels of total phenolic and flavonoid compounds are likely responsible for these bioactivities. These findings highlight the potential of *E. guineensis* extract as a natural source of therapeutic agents for managing oxidative stress, diabetes, and bacterial infections. Further research should focus on isolating the individual bioactive compounds responsible for these effects and assessing their efficacy in clinical trials (“antidiabetic and antimicrobial properties of *E. guineensis* extracts”).

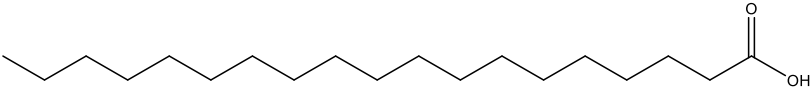
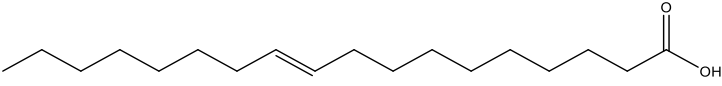
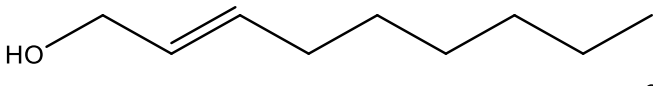
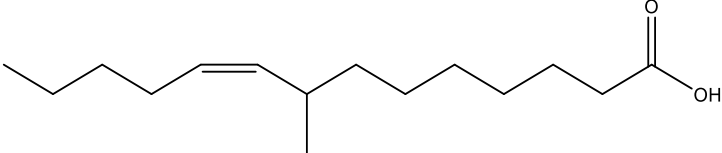
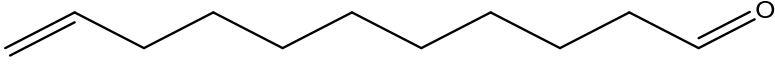
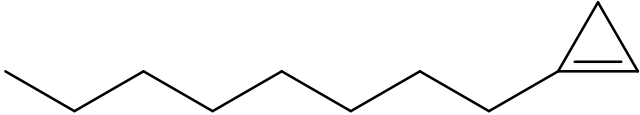
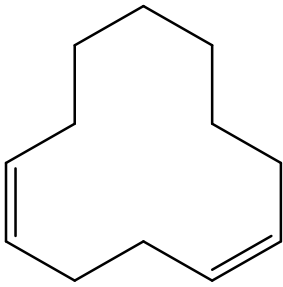
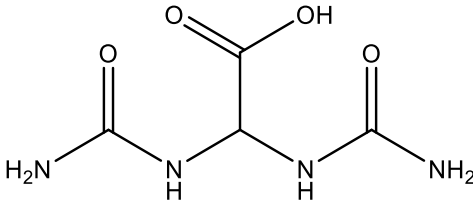
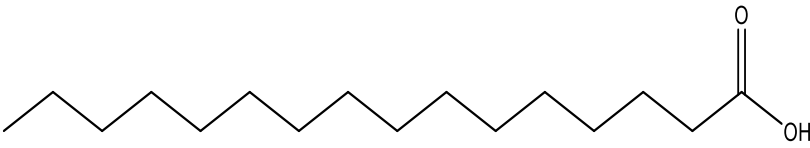
3.3. Chemical composition identified by GC-MS

The biological effect of ethanol peel extract proved to be the strongest of all four solvents examined. Testing by GC-MS helped identify the chemical compounds present in ethanol extracted solvent and enabled molecular docking studies to reveal its underlying mechanism of action. The peel ethanol extract was analyzed using a hybrid analysis tool which combines the resolving powers of a gas-liquid column and detectability of mass spectrometry. Mass spectrometry was employed to verify the existence of compounds in the extract, since it exhibited significant activity (Table 2). Chemical composition is, in a significant part, determined by metabolite polarity, presence of chemicals, the extraction solvents, and extraction techniques [9]. The composition of compounds in extracts is influenced by several factors, including temperature, geographical location, plant variety, freshness, duration of drying, and the method of extraction. The compounds were docked with molecular docking in an attempt to comprehend their impact towards the plant extract’s overall bioactivity. Behavior evaluation of binding is critical for rationally developing small compounds and processes in living organisms.

Table 2. Chemical composition of *E. guineensis*. The area values indicate the relative peak areas derived from the GC-MS total ion chromatogram (TIC). Only significant compounds exhibiting a library match similarity of 90% or greater are included in this report. The cumulative area of the compounds mentioned constitutes 37.85% of the overall chromatogram.

S/ N	Area %	Compound	Molecular structure
1	4.234	9-Octadecenoic acid, (E)	
2	1.230	Oleic Acid	
3	4.891	Naphthalene, 2,7-dimethyl-	
4	1.765	Hydroquinone	
5	2.812	Alpha-L-Glucopyranoside	
6	1.876	Methyl hexofuranoside	

Continued on next page

S/ N	Area %	Compound	Molecular structure
7	2.867	n-Nonadecanoic acid	
8	3.989	10-Octadecenoic acid	
9	0.875	2-Nonen-1-ol	
10	1.321	Z-8-Methyl-9-tetradecenoic acid	
11	3.321	10-Undecenal	
12	2.321	1-octylcycloprop-1-ene	
13	1.497	1,5-Cyclododecadiene	
14	3.865	Allantoic acid	
15	0.989	n-Hexadecanoic acid	

3.4. Virtual docking with DNA gyrase of *S. Typhi*

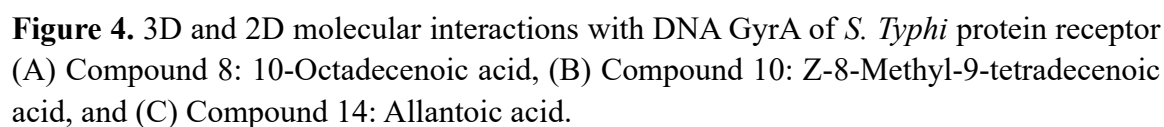
Molecular docking has emerged as a significant computational simulation tool in drug development because it aids in the identification and prediction of efficient ligand poses in a protein's binding pocket as well as the affinity between them [13]. The lack of DNA gyrase in complex eukaryotes makes it a good target for designing antimicrobial compounds that might be lead (s) for

novel antibiotics [9,10,23]. Additionally, the blind docking of the small ligand molecules with *S. Typhi* Gyr A has been reported to enable them to search for an efficient binding site on the protein [8,11]. Validation was conducted by redocking ciprofloxacin, achieving an RMSD of less than 2.0 Å, thereby confirming the accuracy of the docking process. The virtual screening of the ligands with the DNA gyrA chain of *S. Typhi* revealed that the identified compounds 8, 10, and 14 (10-Octadecenoic acid, Z-8-Methyl-9-tetradecenoic acid, and Allantoic acid) have better amino acid residual interactions with the targeted protein (with MolDock scores of between −106.05 and −108.94 kcal/mol) as compared to ciprofloxacin (MolDock score of −105.84 kcal/mol) in Table 3.

Table 3. Binding scores of the identified compounds with DNA GyrA of *S. Typhi*.

Compound No.	MolDock Score (kcal/mol)	Rerank Score	HBond (kcal/mol)
1	−78.32	−64.90	0.00
2	−37.55	−31.62	−5.24
3	−62.48	−53.56	−2.05
4	−58.38	−50.02	−6.45
5	−57.46	−57.18	−13.16
6	−78.99	−53.65	−7.55
7	−104.40	−84.59	−3.24
8	−106.05	−76.05	−5.31
9	−74.97	−62.28	−2.50
10	−107.36	−86.74	−4.33
11	−84.86	−69.85	0.00
12	−78.82	−64.70	0.00
13	−78.75	−59.17	0.00
14	−108.94	−70.56	−8.83
15	−103.28	−78.84	−1.29
Ciprofloxacin	−105.84	−81.90	−5.37

The residues of amino acids involved in the molecular interactions include ARG A: 580, ASP A: 579, LEU A: 581, ILE A: 634, ARG A: 838, GLN A: 788, LEU A: 836, VAL A: 787, ARG A: 630, HIS A: 545, ILE A: 631, SER A: 544. Compound 14 (Allantoic acid), with the highest MolDock score of −108.94 kcal/mol recorded the highest hydrogen bond energy of −8.83 kcal/mol which is depicted as the best and most stable protein-ligand complex amongst others. The most stable docking pose of the selected ligands 8, 10, and 14 with the GyrA subunit protein of *S. Typhi* is presented in Figure 4. While certain compounds exhibited MolDock scores that were near those of ciprofloxacin (approximately 1–



3.5. MD simulation analysis of top compounds

The dynamics simulations were conducted on three selected compounds, namely Compound 8 (10-Octadecenoic acid), Compound 10 (Z-8-Methyl-9-tetradecenoic acid), and Compound 14 (Allantoic acid), all of which formed low binding energy ligand-protein complexes during our docking studies. The RMSD of the protein C α atoms was analyzed to monitor the stability of the complexes over time. RMSD indicates the average deviation of atomic positions from their initial coordinates, offering insight into the system's equilibrium state during the simulation. For a system to be in equilibrium, the RMSD value of the protein's alpha carbons should remain below 3 Å. Higher RMSD values signal greater conformational changes in the system. A steady, flat RMSD slope throughout the simulation suggests system stability, while large fluctuations in the RMSD graph indicate potential instability and weak or unstable ligand binding to the target protein. In all three complexes, 8-5ZTJ, 10-5ZTJ, and 14-5ZTJ, an initial rising trend in RMSD was observed until approximately 100 ns, during which none of the frames exhibited fluctuations exceeding 2.5 Å (Figure 5). This suggests that the systems equilibrate without significant structural instability. Following this phase, the 10-5ZTJ and 14-5ZTJ complexes exhibited minor fluctuations but remained stable throughout the remainder of the simulation, reaching the 200 ns mark without significant changes in RMSD values. In contrast, the 8-5ZTJ complex showed a minor drift in RMSD between 168 ns and 187 ns, after which it regained stability with an RMSD value of approximately 2 Å. The average RMSD values for the 8-5ZTJ, 10-5ZTJ, and 14-5ZTJ complexes were 1.84 Å, 2.22 Å, and 1.89 Å, respectively, reflecting the overall stability of these systems during the 200 ns simulation.

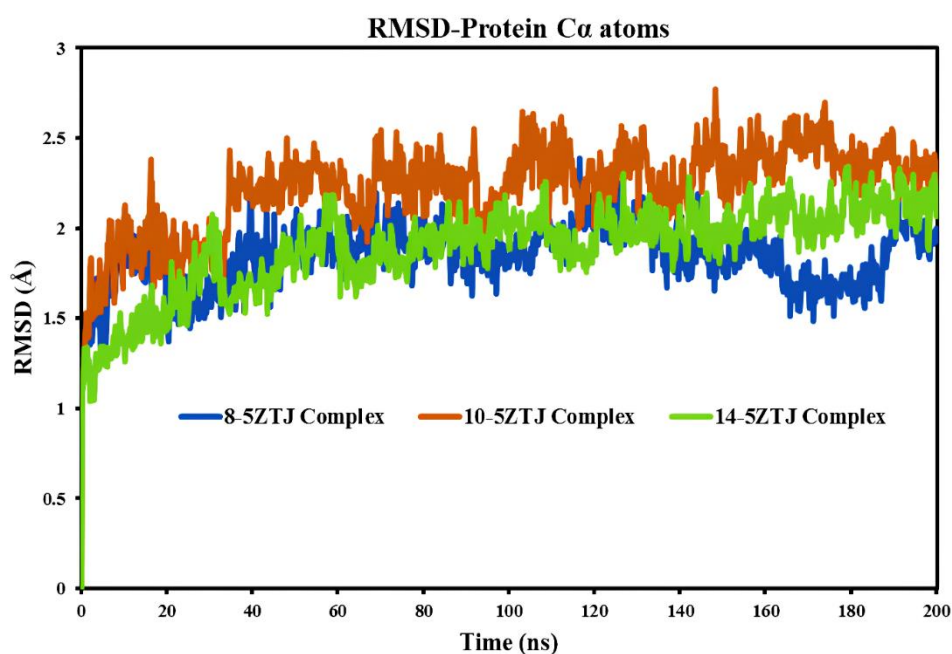


Figure 5. Time-dependent RMSD of C α atoms of *S. Typhi* GyrA (PDB ID: 5ZTJ) protein in complex with Compound 8 (10-Octadecenoic acid), Compound 10 (Z-8-Methyl-9-tetradecenoic acid), and Compound 14 (Allantoic acid).

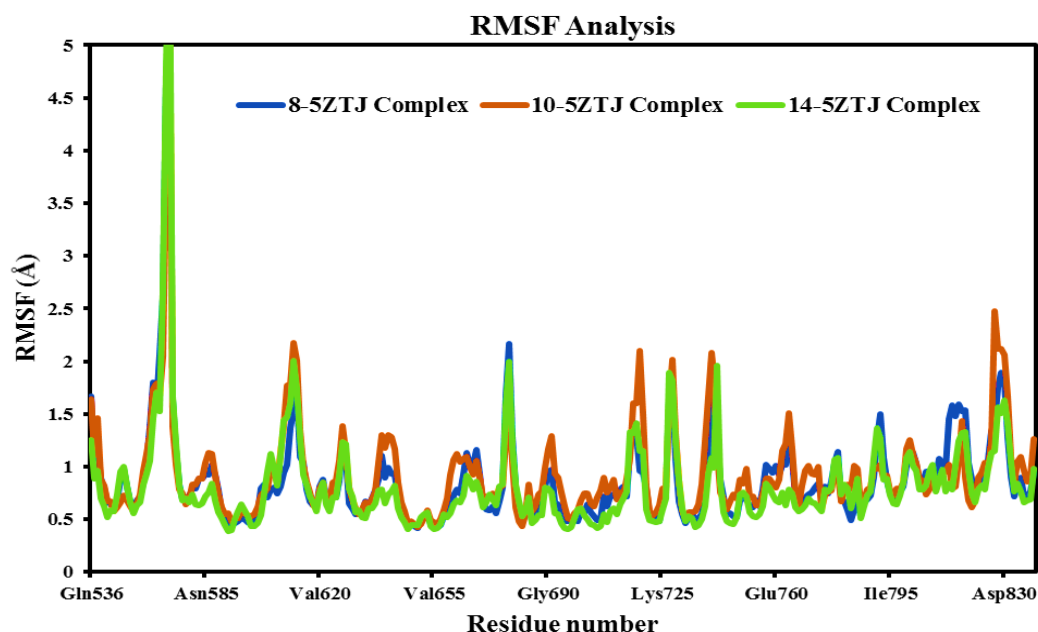


Figure 6. Individual Amino acid residues of *S. Typhi* GyrA (PDB ID: 5ZTJ) protein in complex with Compound 8 (10-Octadecenoic acid), Compound 10 (Z-8-Methyl-9-tetradecenoic acid), and Compound 14 (Allantoic acid).

In addition to RMSD, the RMSF values were calculated to assess the flexibility of individual residues in the protein across all complexes. This analysis is crucial for identifying regions within the protein that exhibit significant movement, as such flexibility could directly influence ligand binding and overall complex stability [40,41]. According to Figure 6, higher RMSF values were observed in the glu558-glu575 region, while all compounds exhibited RMSF values below 2.5 Å. Among the three complexes, the 14-5ZTJ complex exhibited the highest maximum RMSF value of 6.28 Å, followed by the 10-5ZTJ and 8-5ZTJ complexes, with maximum values of 5.84 Å and 5.38 Å, respectively. These peaks likely correspond to flexible regions of the protein, such as terminal residues or loop regions, which tend to be more dynamic; however, this region is not involved in ligand binding. The average RMSF values across the complexes were relatively low, with the 14-5ZTJ complex showing the smallest average RMSF of 0.82 Å, indicating overall stable residue-level dynamics. The 10-5ZTJ and 8-5ZTJ complexes had slightly higher average RMSF values of 0.94 Å and 0.88 Å, respectively, which fall within a stable range, suggesting minimal residue-level perturbation. The minimum RMSF values across all complexes were nearly identical, around 0.39–0.42 Å, reflecting the stability of core regions within the protein. Overall, the RMSF data aligns with the RMSD results, supporting the conclusion that all three complexes maintain stable binding interactions with localized flexibility that does not significantly impact overall complex stability.

Hydrogen bond analysis in MD simulations plays a crucial role in assessing ligand-protein binding stability and affinity. Stable and consistent hydrogen bonds indicate strong, high-affinity interactions between the ligand and the protein, suggesting more effective binding. The number and duration of these bonds help determine the overall stability of the complex, with more stable hydrogen bonds correlating to a higher binding affinity [3,42,43]. This analysis provides valuable insights into the potential of a compound as a drug or inhibitor, aiding the selection of promising candidates for

further experimental validation and drug development. For the 8-5ZTJ complex, the hydrogen bond data showed a minimum of 1 bond, a maximum of 3 bonds, and an average of 1.57, indicating a relatively stable but moderate interaction between the ligand and the protein.

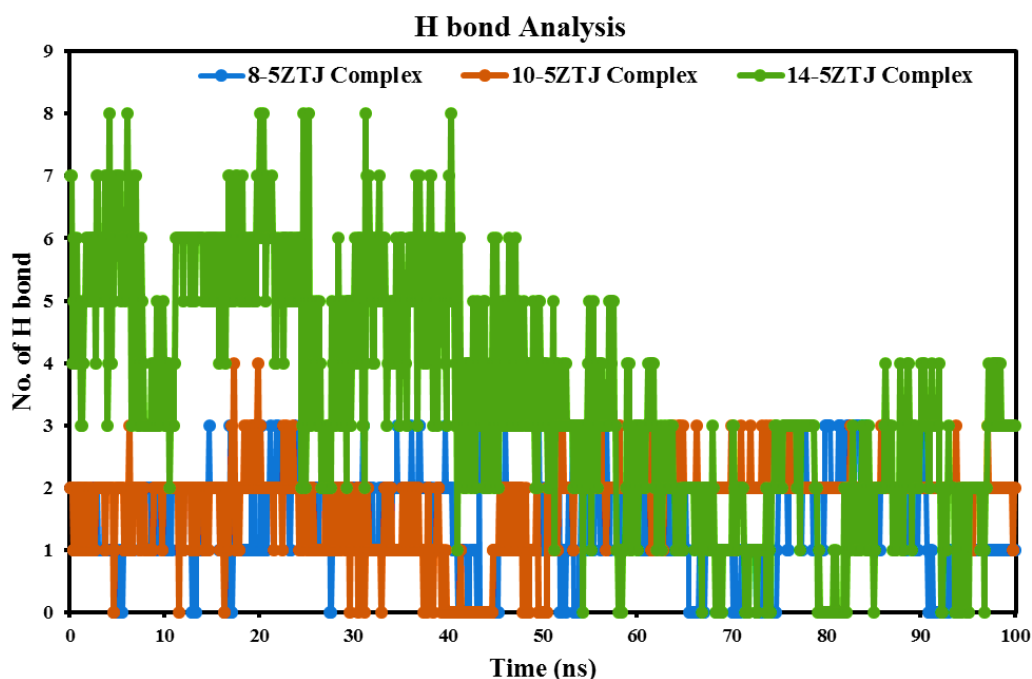


Figure 7. Time-dependen Hydrogen bond analysis of Compound 8 (10-Octadecenoic acid), Compound 10 (Z-8-Methyl-9-tetradecenoic acid), and Compound 14 (Allantoic acid) in complex with *S. Typhi* GyrA (PDB ID: 5ZTJ) protein.

The 10-5ZTJ complex also had a minimum of 1 hydrogen bond, but the maximum increased to 4, with an average of 2.01, suggesting slightly stronger and more dynamic hydrogen bonding compared to the 8-5ZTJ complex. The 14-5ZTJ complex exhibited a wider range of hydrogen bonds, with a minimum of 1 and a maximum of 8, and an average of 1.94, reflecting a more variable interaction profile. The higher maximum number of hydrogen bonds in the 14-5ZTJ complex may suggest more dynamic or transient hydrogen bonds during the simulation, potentially contributing to greater flexibility in ligand binding (Figure 7). This could be attributed to the structural characteristics of Compound 14 (Allantoic acid), which possesses several polar groups, such as amines, hydroxyls, and carboxyls, capable of engaging in hydrogen bonding with the protein's amino acid residues, especially those with donor and acceptor sites like serine, threonine, asparagine, or glutamine. Overall, the RMSD, RMSF, and hydrogen bond analyses demonstrate the binding stability of Compounds 8, 10, and 14 within the *S. Typhi* GyrA (PDB ID: 5ZTJ), highlighting stable ligand-protein interactions with varying levels of dynamic flexibility, suggesting that all three complexes maintain overall stability, with Compound 14 exhibiting more dynamic binding characteristics.

3.6. Antibacterial efficacy prediction (*in-silico*)

The assessment of antibacterial activity revealed that the 15 compounds derived from *E.*

guineensis displayed an inhibitory effect on 47 bacterial species, with a *Pa* value exceeding 0.5, as detailed in Figure 8 and Supplemental Information (Table S1). Notably, the bacterial strains *Y. pestis* and *Actinomyces meyeri* were significantly impacted by 6 and 4 of the phytochemicals, respectively. Among these, Alpha-L-Glucopyranoside and 1-octylcycloprop-1-ene exhibited the highest antibacterial efficacy, with *Pa* values greater than 0.9 against *Y. pestis* and *Streptococcus sp.* In the context of *S. typhi*, the bacterial strain utilized in our *in-vitro* analysis, 6 out of the 15 compounds were predicted to exert an inhibitory effect. This pronounced inhibitory activity indicates that *E. guineensis* extracts could potentially function as effective antibacterial agents. The zones of inhibition exhibiting antibacterial properties for *S. Typhi* (Table 1 and Figure 3) demonstrate effects at the extract level, while Fig. 8 illustrates the anticipated probabilities at the compound level across various bacteria. Consequently, variations are anticipated and may indicate limitations in diffusion as well as interactions between compounds within the extract.

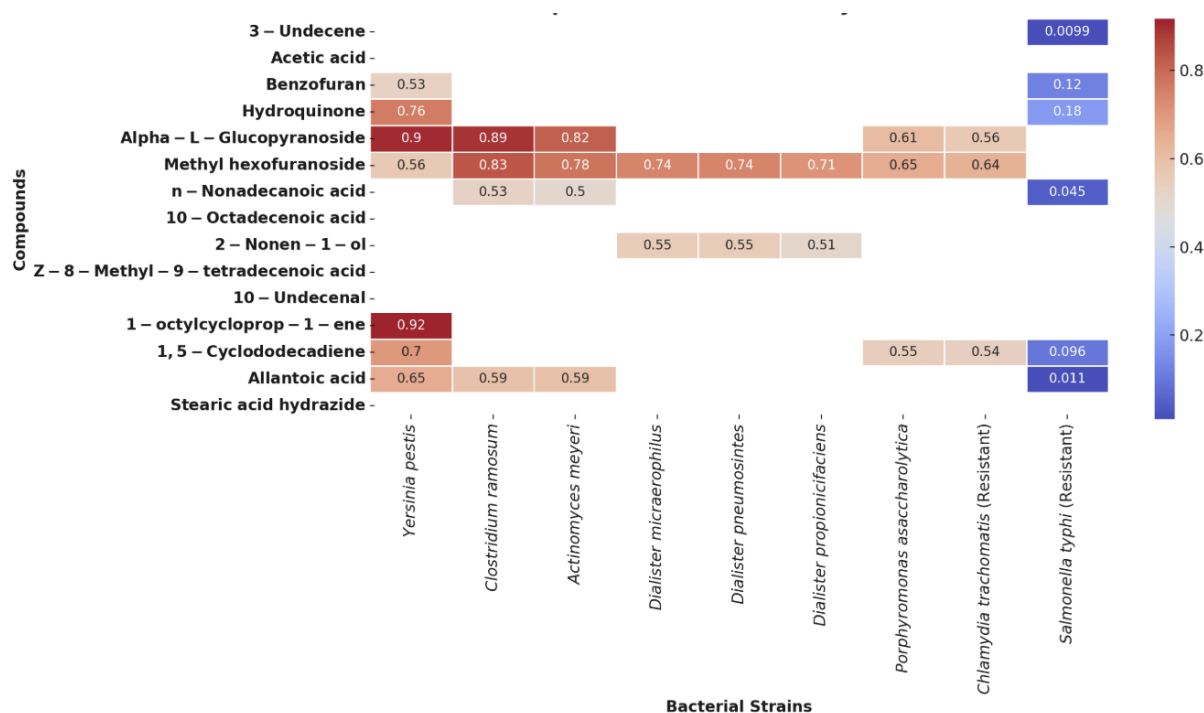


Figure 8. Antibacterial activity of chemical compounds against selected bacterial strains. The gradient of colors conveys the confidence score, with red tones indicating a greater antibacterial efficacy, whereas blue tones suggest a lesser antibacterial efficacy.

3.7. ADMET properties of selected ligands

The poor pharmacokinetics and toxicity are responsible for many occurrences of drug attrition during the later phases of drug development [44,45]. As a result, early evaluation of ADMET is critical for developing novels leading to medicinal candidates. The top virtually screened compounds 8, 10, and 14 were predicted to exhibit favorable ADMET properties relative to ciprofloxacin as presented in Table 4. Moreover, the three selected phytochemicals are predicted to be non- substrate for Pgp (P-glycoprotein) and are therefore easily absorbed compared with ciprofloxacin. Only Compound 14 was predicted to be a non-inhibitor and substrate of cytochrome P450, which is quite similar to

ciprofloxacin. In addition, Compound 14 was predicted to have a better ADMET profile, with the acceptable toxicity indicators (carcinogenicity, respiratory toxicity, drug-induced liver damage, and human hepatocyte toxicity), showing the compound's desirable properties in comparison with ciprofloxacin as the standard drug.

To ensure meaningful biological interpretations of the ADMET properties, the results were contextualized against established pharmacological thresholds (Table 4). Probability bands defined by ADMETLab ($- \leq 0.3$ “negative”, $+ 0.5-0.7$ “possible”, $++ 0.7-0.9$ “likely”, $+++ \geq 0.9$ “very likely”) were utilized as benchmarks to portrays the liabilities and strengths. The absorption and distribution analysis revealed a consistent strength across all three selected phytocompounds with their predicted non-substrate status for P-gp efflux pumps ($-$), compared to ciprofloxacin (P-gp substrate $+++$). This suggested a reduced risk of intestinal efflux and potentially improved oral bioavailability compared with the reference drug. Furthermore, the uniformly negative prediction for BBB penetration ($-$) suggests these compounds are less likely to cross into the central nervous system, which is generally desirable for antibacterial to minimize off-target neurological effects. In the metabolism and drug-drug interaction (DDI) liability assessment, Compounds 8 and 10 exhibit broad multi-CYP inhibition potentials (e.g., Compound 8: CYP1A2, CYP2C9, CYP2C19 $+++$; Compound 10: CYP2C9 $++$, CYP2C19 substrate $++$), raising a red flag for potential drug–drug interactions if co-administered with other therapeutics metabolized by these enzymatic isoforms. Hence, Compound 14 was predicted as the “cleanest” metabolizer with both non-inhibitory and non-substrate potentials across the major CYP families, which have minimal metabolic liabilities and aligns with favorable pharmacokinetic behavior. The excretion and systemic exposure prediction results suggest that Compound 14 has a longer half-life (2.29) and lower clearance (1.154) when compared with Compounds 8 ($t_{1/2}$ 0.847; CL 3.452), 10 ($t_{1/2}$ 0.672; CL 3.621), and even ciprofloxacin ($t_{1/2}$ 1.563; CL 3.313).

Interestingly, all three phytocompounds displayed low hERG blocker probabilities (≤ 0.115), substantially reducing the risk of drug-induced arrhythmias for cardiac and hepatic safety. It is worthy to note that the same Compound 14 showed the lowest hERG liability (0.012), thereby outperforming ciprofloxacin (0.105). Additionally, the hepatotoxicity predictions further suggests that Compound 14 again scored lowest (0.111), implying a reduced risk of drug-induced liver injury in comparison with Compound 8 (0.681) and ciprofloxacin (0.983). These findings reinforce Compound 14 as the safest candidate in terms of cardiac and hepatic endpoints. As for other toxicological metrics, all three selected phytocompounds were predicted to have high eye-irritation probabilities (> 0.97), which represents a potential local safety concern requiring targeted experimental evaluation. The respiratory toxicity was strongly predicted for Compound 8 (0.933) and ciprofloxacin (0.999), moderately for Compound 10 (0.691), and only weakly for Compound 14 (0.232), further positioning Compound 14 as the most balanced candidate. In addition, the carcinogenicity scores for all compounds remained low (≤ 0.258), well below thresholds of concern.

PASS indicated significant antibacterial efficacy for Compounds 5 and 12, whereas the ADMET analysis of Compound 14 revealed encouraging pharmacokinetic properties. These computational results enhance the experimental antimicrobial effects noted *in-vitro*, implying that components may work together synergistically. These identified phyto-compounds might be responsible for the fascinating bioactivities of the extracts. However, allantoin acids had a better and positive ADMET profile and could be further utilized for drug optimization.

Table 4. ADMET profiles of the top selected compounds.

Category	Properties	Prediction probability values (symbols)			
Absorption		8	10	14	Ciprofloxacin
	Caco-2 Permeability	−5.08	−5.121	−6.092	−5.863
	Pgp-inhibitor	---	---	---	---
	Pgp-substrate	---	---	---	+++
	Human Intestinal Absorption	--	---	---	---
Distribution	Volume distribution	−0.758	−0.629	−0.466	0.262
	BBB penetration	---	---	---	---
Metabolism	CYP1A2 inhibitor	+++	--	---	---
	CYP1A2 substrate	---	---	---	---
	CYP2C19 inhibitor	+++	---	---	---
	CYP2C19 substrate	---	++	---	---
	CYP2C9 inhibitor	+++	++	---	---
	CYP2C9 substrate	+++	+++	---	---
	CYP2D6 inhibitor	++	---	---	---
	CYP2D6 substrate	+++	-	---	---
	CYP3A4 inhibitor	---	---	---	---
	CYP3A4 substrate	---	---	---	---
Excretion	Clearance level	3.452	3.621	1.154	3.313
	Half-life	0.847	0.672	2.29	1.563
Toxicity	Carcinogenicity	0.087	0.075	0.258	0.191
	Eye Irritation	0.992	0.994	0.977	0.215
	Respiratory toxicity	0.933	0.691	0.232	0.999
	hERG Blockers	0.081	0.115	0.012	0.105
	Human Hepatotoxicity	0.681	0.276	0.111	0.983
	Rat Oral Acute Toxicity	0.042	0.06	0.056	0.743
	FDAMDD	0.211	0.133	0.02	0.481

Key: The prediction probability symbols: (0–0.1), “--” (0.1–0.3), “-” (0.3–0.5), “+” (0.5–0.7), “++” (0.7–0.9), and “+++” (0.9–1.0). Green color; excellent/favorable, yellow; medium, red; poor/discoverable.

The antioxidant, α -glucosidase inhibition, and antimicrobial properties of *E. guineensis* extracts can be attributed to its high phenolic and flavonoid content. These bioactivities suggest its potential as a natural therapeutic agent for managing oxidative stress, diabetes, and bacterial infections. Furthermore, the *in-silico* study reveals that three identified compounds (10-Octadecenoic acid; Z-8-Methyl-9-tetradecenoic acid; and Allantoic acid) bind protein of *S. Typhi* with DNA gyrA more efficiently than a standard drug.

4. Conclusions

In terms of alpha-glucosidase inhibitory activity, total phenolic compounds, reducing power,

radical scavenging, and antibacterial activities, the ethanol peel extract showed strong antioxidant activity. Some of the compounds from the ethanol peel extract of *E. guineensis* function as possible *S. Typhi* inhibitors, according to the molecular docking tool. The virtual docking screening showed that, Compounds 8, 10, and 14 have better binding scores with MolDock scores between -106.05 and -108.94 kcal/mol than that of ciprofloxacin (-105.84 kcal/mol) with hydrogen and hydrophobic bonds playing the most crucial contributions in the molecular interactions. Researchers should aim to analyze 10-Octadecenoic acid, Z-8-Methyl-9-tetradecenoic acid and Allantoic acid effects *in vivo* as well as in clinical trials.

Use of generative-AI tools declaration

The authors declare they have not used Artificial Intelligence (AI) tools in the creation of this article.

Conflict of interest

The authors declare no conflict of interest.

Author contributions

All authors were involved in developing and designing the study. AMD AAL AAM MU and performed the *in-vitro* study. AAA, AA-RM, MTI and MA performed the *in-silico* study. All the authors read and approved the final manuscript.

References

1. Reygaert WC (2018) An overview of the antimicrobial resistance mechanisms of bacteria. *AIMS Microbiol* 4: 482–501. <https://doi.org/10.3934/microbiol.2018.3.48>
2. Abdullahi M, Uzairu A, Shallangwa GA, et al. (2024) Modelling of novel bornoel analogs as Influenza A Virus inhibitors through genetic function approximation, comparative molecular fields, molecular docking, and ADMET/Pharmacokinetic studies. *Intell Pharm* 2: 190–203. <https://doi.org/10.1016/j.ipha.2023.11.004>
3. Jedli O, Ben-Nasr H, Zammel N, et al. (2022) Attenuation of ovalbumin-induced inflammation and lung oxidative injury in asthmatic rats by Zingiber officinale extract: Combined in silico and in vivo study on antioxidant potential, STAT6 and TNF- α pathways. *3 Biotech* 12: 191. <https://doi.org/10.1007/s13205-022-03249-5>
4. Lim T (2011) *Elaeis guineensis*, *Edible Medicinal and Non-Medicinal Plants*, Springer, 335–392. https://doi.org/10.1007/978-90-481-8661-7_46
5. Erinoso SM, Aworinde DO, Teniola OA, et al. (2020) Ethnobotany of *Elaeis guineensis* Jacq. and its importance in the household economy of the Ikale and Ilaje of Ondo State, Nigeria. *Ethnobotany Res Appl* 20: 1–16. <http://dx.doi.org/10.32859/era.20.42.1-16>
6. Enebeli-Ekwutoziam KC, Aruah CB, Ogbonna BO, et al. (2021) A review of ethnomedicinal plant resources in southern Nigeria. *Ethnobotany Res Appl* 22: 1–40. <http://dx.doi.org/10.32859/era.22.13.1-40>

7. Limmongkon A, Janhom P, Amthong A, et al. (2017) Antioxidant activity, total phenolic, and resveratrol content in five cultivars of peanut sprouts. *Asian Pac J Trop Bio* 7: 332–338. <https://doi.org/10.1016/j.apjtb.2017.01.002>
8. Maliszewski D, Demirel R, Wróbel A, et al. (2023) s-Triazine derivatives functionalized with alkylating 2-chloroethylamine fragments as promising antimicrobial agents: Inhibition of bacterial DNA gyrases, molecular docking studies, and antibacterial and antifungal activity. *Pharmaceuticals* 16: 1248. <https://doi.org/10.3390/ph16091248>
9. Khan T, Sankhe K, Suvarna V, et al. (2018) DNA gyrase inhibitors: Progress and synthesis of potent compounds as antibacterial agents. *Biomed Pharm* 103: 923–938. <https://doi.org/10.1016/j.biopha.2018.04.021>
10. Dighe SN, Collet TA (2020) Recent advances in DNA gyrase-targeted antimicrobial agents. *Eur J Med Chem* 199: 112326. <https://doi.org/10.1016/j.biopha.2018.04.021>
11. Adetutu A, Olaniyi TD, Owoade OA (2021) GC-MS analysis and in silico assessment of constituents of Psidium guajava leaf extract against DNA gyrase of Salmonella enterica serovar Typhi. *Informatics Med Unlocked* 26: 100722. <https://doi.org/10.1016/j.imu.2021.100722>
12. Pradhan T, Gupta O, Singh G, et al. (2021) Aurora kinase inhibitors as potential anticancer agents: Recent advances. *Eur J Med Chem* 221: 113495. <https://doi.org/10.1016/j.ejmech.2021.113495>
13. Muhammed MT, Aki-Yalcin E (2024) Molecular docking: principles, advances, and its applications in drug discovery. *Lett Drug Des Discov* 21: 480–495. <https://doi.org/10.2174/1570180819666220922103109>
14. Abdulrahman MD, Hamad SW (2022) Traditional methods for treatment and management of measles in Northern Nigeria: Medicinal plants and their molecular docking. *Ethnobotany Res Appl* 23:1–18. <http://dx.doi.org/10.32859/era.23.33.1-18>
15. Zhao C, Yang C, Wai STC, et al. (2019) Regulation of glucose metabolism by bioactive phytochemicals for the management of type 2 diabetes mellitus. *Crit Rev Food Sci* 59: 830–847. <https://doi.org/10.1080/10408398.2018.1501658>
16. Panche AN, Diwan AD, Chandra SR (2016) Flavonoids: an overview. *J Nutr Sci* 5: 1–15. <http://dx.doi.org/10.1017/jns.2016.41>
17. Faramayuda F, Windyaswari AS, Karlina Y, et al. (2024) Effect of extraction method on antioxidant activity of palm palm leaves (*Elaeis guineensis* jacq.). *Med Sains: Jurnal Ilmiah Kefarmasian* 9: 67–76. <https://doi.org/10.37874/ms.v9i1.994>
18. Ai L, Liu L, Zheng L, et al. (2024) An on-line stop-flow RPLC× SEC-MS/DPPH radical scavenging activity analysis system and its application in separation and identification of antioxidant peptides. *Food Chem* 436: 137670. <https://doi.org/10.1016/j.foodchem.2023.137670>
19. Ouattara N, Magid AA, Escotte-Binet S, et al. (2024) Anti-toxoplasma gondii screening of eight species and bio-guided identification of metabolites of *Elaeis guineensis* leaves, a preliminary study. [bioRxiv:2024.06.24.600452](https://doi.org/10.1101/2024.06.24.600452). <https://doi.org/10.1101/2024.06.24.600452>
20. Bentivenga GM, Mammana A, Baiardi S, et al. (2024) Performance of a seed amplification assay for misfolded alpha-synuclein in cerebrospinal fluid and brain tissue in relation to Lewy body disease stage and pathology burden. *Acta Neuropathol* 147: 18. <https://doi.org/10.1007/s00401-023-02663-0>
21. Daliri SO (2024) Investigation of antimicrobial effect and mechanical properties of modified starch films, cellulose nanofibers, and citrus essential oils by disk diffusion method. *Asian J Green Chem* 7: 1–14.

22. Abdulrahman MD, Hasan Nudin NF, Khandaker MM, et al. (2019) In vitro biological investigations on *Syzygium polyanthum* cultivars. *Int J Agric Biol* 22: 1399–1406. <https://doi.org/10.17957/IJAB/15.1214>
23. Salman M, Sharma P, Kumar M, et al. (2023) Targeting novel sites in DNA gyrase for development of anti-microbials. *Brief Funct Genomics* 22: 180–194. <https://doi.org/10.1093/bfgp/elac029>
24. Poleboyina PK, Naik U, Pasha A, et al. (2024) Virtual screening, molecular docking, and dynamic simulations revealed TGF- β 1 potential inhibitors to curtail cervical cancer progression. *Appl Biochem Biotech* 196: 1316–1349. <https://doi.org/10.1007/s12010-023-04608-5>
25. Abdullahi M, Uzairu A, Shallangwa GA, et al. (2023) Molecular modelling studies of substituted indole derivatives as novel influenza A virus inhibitors. *J Biomol Struct Dyn* 41: 1–20. <https://doi.org/10.1080/07391102.2023.2280735>
26. Siddiqui AJ, Jamal A, Zafar M, et al. (2024) Identification of TBK1 inhibitors against breast cancer using a computational approach supported by machine learning. *Front Pharm* 15: 1342392. <https://doi.org/10.3389/fphar.2024.1342392>
27. Jahan S, Redhu NS, Siddiqui AJ, et al. (2022) Nobiletin as a neuroprotectant against NMDA receptors: an in silico approach. *Pharmaceutics* 14: 1123. <https://doi.org/10.3390/pharmaceutics14061123>
28. Siddiqui AJ, Badraoui R, Jahan S, et al. (2023) Targeting NMDA receptor in Alzheimer's disease: identifying novel inhibitors using computational approaches. *Front Pharm* 14: 1208968. <https://doi.org/10.3389/fphar.2023.1208968>
29. Siddiqui AJ, Kumar V, Jahan S, et al. (2023) Computational insight into structural basis of human ELOVL1 inhibition. *Comput Biol Med* 157: 106786. <https://doi.org/10.1016/j.combiomed.2023.106786>
30. Surti M, Patel M, Adnan M, et al. (2020) Ilimaquinone (marine sponge metabolite) as a novel inhibitor of SARS-CoV-2 key target proteins in comparison with suggested COVID-19 drugs: designing, docking and molecular dynamics simulation study. *RSC Adv* 10: 37707–37720. <https://doi.org/10.1039/D0RA06379G>
31. Abdullahi M, Uzairu A, Shallangwa GA, et al. (2023) Structure-based drug design, molecular dynamics simulation, ADMET, and quantum chemical studies of some thiazolinones targeting influenza neuraminidase. *J Biomol Struct Dyn* 41: 13829–13843. <https://doi.org/10.1080/07391102.2023.2208225>
32. Filimonov D, Lagunin A, Gloriovova T, et al. (2014) Prediction of the biological activity spectra of organic compounds using the PASS online web resource. *Chem Heterocycl Com* 50: 444–457. <https://doi.org/10.1007/s10593-014-1496-1>
33. Zhong Y, Yang Y, Xu Y, et al. (2024) Design of a Zn-based nanozyme injectable multifunctional hydrogel with ROS scavenging activity for myocardial infarction therapy. *Acta Biomater* 177: 62–76. <https://doi.org/10.1016/j.actbio.2024.01.015>
34. Krishnaiah D, Sarbatly R, Nithyanandam R (2011) A review of the antioxidant potential of medicinal plant species. *Food Bioprod Process* 89: 217–233. <https://doi.org/10.1016/j.fbp.2010.04.008>
35. Alhaji AM, Almeida ES, Carneiro CR, et al. (2024) Palm oil (*Elaeis guineensis*): A journey through sustainability, processing, and utilization. *Foods* 13: 2814. <https://doi.org/10.3390/foods13172814>

36. Shahidi F, Ambigaipalan P (2015) Phenolics and polyphenolics in foods, beverages and spices: Antioxidant activity and health effects—A review. *J Funct Foods* 18: 820–897. <https://doi.org/10.1016/j.jff.2015.06.018>
37. Stanislaus O, Etsuyankpa M, Tanko O (2022) Antibacterial activities of selected medicinal plants against *Salmonella typhi*, *Salmonella paratyphi* A, B and C, clinical isolates in North Central, Nigeria. *Afr J Biotechnol* 21: 528–538. <https://doi.org/10.5897/AJB2021.17363>
38. Mahmood M, Ashraf A, Ali S, et al. (2021) Portrayal of *Punica granatum* L. peel extract through High Performance Liquid Chromatography and antimicrobial activity evaluation. *Braz J Biol* 83: e244435. <https://doi.org/10.1590/1519-6984.244435>
39. Cushnie TT, Lamb AJ (2005) Antimicrobial activity of flavonoids. *Int J Antimicrob Agents* 26: 343–356. <https://doi.org/10.1016/j.ijantimicag.2005.09.002>
40. Siddiqui AJ, Badraoui R, Alshahrani MM, et al. (2024) A computational and machine learning approach to identify GPR40-targeting agonists for neurodegenerative disease treatment. *Plos One* 19: e0306579. <https://doi.org/10.1371/journal.pone.0306579>
41. Abdullahi M, Uzairu A, Shallangwa GA, et al. (2023) In-silico molecular modelling studies of some camphor imine based compounds as anti-influenza A (H1N1) pdm09 virus agents. *J Biomol Struct Dyn* 41: 1–21. <https://doi.org/10.1080/07391102.2023.2209654>
42. Abdullahi M, Uzairu A, Shallangwa GA, et al. (2023) Modelling of novel bornoel analogs as Influenza A Virus inhibitors through genetic function approximation, comparative molecular fields, molecular docking, and ADMET/Pharmacokinetic studies. *Intell Pharm* 2: 190–203. <https://doi.org/10.1016/j.ipha.2023.11.004>
43. Abdullahi M, Uzairu A, Shallangwa GA, et al. (2024) In-silico design of novel 2-((4-chloro-6-methoxy-1H-indol-3-yl)thio)-N-(2-ethoxyphenyl)acetamide derivatives as potential inhibitors of influenza neuraminidase protein receptor. *Intell Pharm* 2: 495–504. <https://doi.org/10.1016/j.ipha.2023.12.002>
44. Ruiz-Garcia A, Bermejo M, Moss A, et al. (2008) Pharmacokinetics in drug discovery. *J Pharm Sci* 97: 654–690. <https://doi.org/10.1002/jps.21009>
45. Parasrampur DA, Benet LZ, Sharma A (2018) Why drugs fail in late stages of development: case study analyses from the last decade and recommendations. *AAPS J* 20: 1–16. <https://doi.org/10.1208/s12248-018-0204-y>



AIMS Press

© 2025 the Author(s), licensee AIMS Press. This is an open access article distributed under the terms of the Creative Commons Attribution License (<http://creativecommons.org/licenses/by/4.0>)